RSC Advances

ROYAL SOCIETY OF CHEMISTRY

www.rsc.org/advances

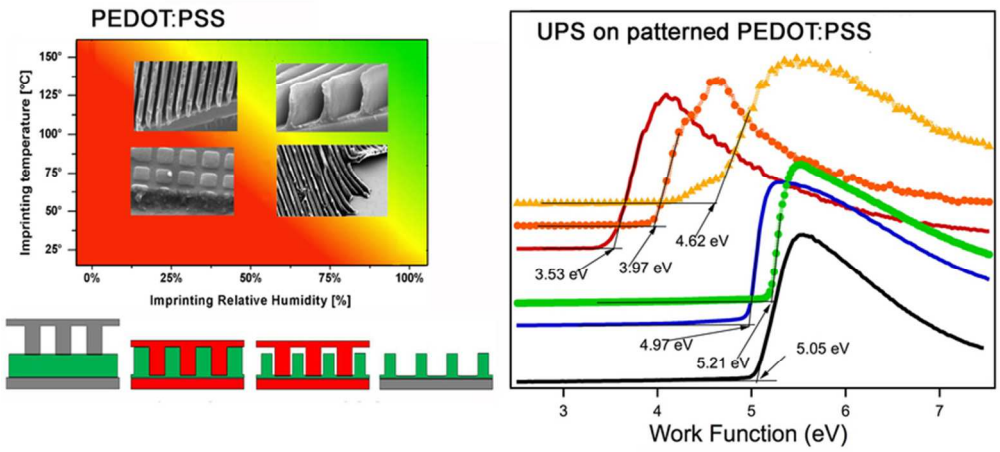

A modified Nanoimprinting Lithography process performed at high relative humidity was developed for high-resolution pattering of the conductive polymer PEDOT:PSS. The process induce important effect on the electronic properties of the material, including enhanced conductivity and strong shifts in the work function and valence band edge.
36x16mm (600 x 600 DPI)

Patterning PEDOT:PSS and Tailoring its Electronic Properties by Water-Vapour-Assisted Nanoimprint Lithography

Andrea Radivo[1,2], Enrico Sovernigo[1,3], Marco Caputo[4], Simone Dal Zilio[1], Tsegaye Endale[5], Alessandro Pozzato[3], Andrea Goldoni[4], Massimo Tormen[1,3,*]

[1] Istituto Officina dei Materiali-CNR, Laboratorio TASC, I-34149 Trieste, Italy

[2] University of Trieste, Piazzale Europa, 1, 34127 Trieste, Italia

[3] ThunderNIL srl, via Ugo Foscolo 8, 35131 Padova, Italy

[4] Sincrotrone Trieste SCpA, I-34149 Trieste, Italy

[5] Department of Chemistry, Addis Ababa University, P. O. Box: 1176, Addis Ababa, Ethiopia

* Corresponding author address: Istituto Officina dei Materiali-CNR, Laboratorio TASC, S.S. 14 km 163,5 I-34149 Basovizza (Trieste), Italy, Tel +39 0403758416, email address: tormen@iom.cnr.it

Abstract

We present a new water-vapour-assisted nanoimprint lithography (NIL) process for the patterning of the conducting poly(3,4-ethylenedioxythiophene):poly(styrenesulfonate) (PEDOT:PSS). The process was optimized with respect to relative humidity, applied pressure and temperature (RH, p, T). The control of environmental humidity was found to be crucial. High quality nanostructures were reproducibly obtained at high relative humidity values

(RH ≳75%), with sub-100 nm resolution features attaining aspect ratios as high as ~6 at ~95% RH. The developed process of water-vapour-assisted NIL (WVA-NIL) strongly affects the electronic properties of PEDOT:PSS. By current-voltage measurements and ultraviolet photoemission spectroscopy we demonstrate that the process parameters p, T and RH are correlated with changes of PEDOT:PSS conductivity, work function and states of the valence band. In particular, an increase in the films conductivity by factors as high as 10^5 and a large decrease in the work function, up to 1.5 eV, upon WVA-NIL processing were observed. Employed as anode buffer layer in P3HT:ICBA bulk heterojunction solar cells, PEDOT:PSS processing was found to affect significantly the devices performance.

Keywords: organic solar cells; PEDOT:PSS; nanoimprint lithography; UPS; work function.

1. Introduction

Owing to its huge economic growth potential, organic optoelectronics is a field of intense applied research and a very attractive new market for innovative companies. The development of technologies based on conjugated materials for energy conversion (e.g. photovoltaic cells[1]), energy storage (e.g. supercapacitors[2]), or energy saving (e.g. lighting by OLEDs[3]) is boosted by the prospect of cheap, lightweight, flexible and environmentally friendly devices, produced over large area substrates by high throughput techniques[4,5,6,7,8] as already successfully demonstrated by the market of OLED displays (smartphones, TVs).

The architectures of organic semiconductors based devices are in many cases rather simple. They essentially consist of stacks of planar layers, patterned at the scale of tens to hundreds of micrometres[9] by methods such as ink-jet[10,11] screen printing[12] or laser ablation[13]. The development of organic-based devices is not subject to any roadmap of features' downscaling, analogous to that that in silicon-based microelectronics is referred to as the Moore's law. Nonetheless, new device architectures are calling for an extension to the sub-100 nm scale of the technologies suitable for the patterning of conjugated materials.[14,15,16]

Here we explore the patterning at that scale of poly(3,4-ethylenedioxythiophene):poly(styrenesulfonate) (PEDOT:PSS). The π-conjugated polymer (PEDOT) together with the polyanion (PSS) dispersed in water is currently the most frequently used anode buffer layer on Indium Tin Oxide (ITO) transparent electrode for its relatively high conductivity, high work function, mechanical flexibility, stability, transparency and easy processing in thin films by spin coating, inkjet printing, hair-brushing, doctor blading. PEDOT:PSS is widely used for organic thin-film transistors (OTFTs), organic light-emitting diode (OLED) displays and in organic photovoltaic device (OPV), and has been also demonstrated as catalytically active anti-corrosion electrode in photoelectrochemical cells[17,18], in

ionic charge storage medium for super capacitors,[19,20] or as stable, biocompatible, implantable electrodes for in vivo neuronal activity recording.[21]

PEDOT:PSS, similarly to other anode buffer layers, is introduced so as to i) provide an ohmic contact with p-type organic materials; ii) to transport positive charges efficiently, iii) to block negative charges.[22] In addition it should present low series resistance (Rs) and act as a planarization layer for the often-rough ITO surface, so as to prevent electrical shorts and increase device yield. Moreover, it is very actively investigated as an option to fully replace the expensive ITO.[23,24,25,26,27,28] The improved contacts that PEDOT:PSS provides to most p-type organic semiconductors compared to bare ITO, is usually explained to arise from the PEDOT:PSS higher work function (reported to be between 4.8 and 5.2 eV) versus that of ITO (~4.7 eV). This would thus result in a reduction of the barrier for hole injection from the deep-lying HOMO levels of many conjugated semiconductors.[29,30]

Past investigations have highlighted severe hurdles in nanopatterning PEDOT:PSS by standard lithographic techniques. At the micrometre scale several methods[31] have been successfully applied, such as soft lithography[32], inking and stamping[33], pulsed UV laser patterning[34], ink jet printing, screen printing in roll to roll system[35]. However, extending the previous techniques to the patterning of PEDOT:PSS at the sub-micrometre scale proved to be non-viable.

Therefore, we concentrated most efforts on nanoimprinting lithography (NIL) in spite of the modest success to patterning PEDOT:PSS by this technique to date.[36,16] The main problems of applying the standard NIL protocols to PEDOT:PSS are related to the thermo-mechanical properties of this material. In fact, it decomposes with temperature prior to exhibiting a distinct glass transition, while at room temperature and standard lab condition, due to its strong tendency to water uptake from environmental humidity, the material appears sticky and as having low internal cohesion. This leads to nanostructures prone to being easily damaged or ripped-off from

the substrate during the separation of the stamp (step that we will refer to as "demoulding") at the end of the NIL process.[37] Organic plasticizers, such as sorbitol[38], glycerol[39] have been used to enhance the material flow, yet with partial success.[40,41] PEDOT:PSS is a composite material, with grains consisting of a rigid, conductive and hydrophobic PEDOT-rich core and a hydrophilic, soft and non conductive PSS-rich shell, with electrical and mechanical proprieties that are heavily influenced by the water content. In solution PEDOT clusters are kept in colloidal suspension by the PSS shell, and their size in solution has been shown to depend strongly on temperature and concentration.[42,43] When spin coated the resulting films show a highly anisotropic structure with flattened colloids into PEDOT-rich "lasagne-like" structures separated by PSS-rich lamellas. Water uptake from the atmospheric moisture is for thin PEDOT:PSS film very fast (in the matter of seconds for sub-100 nm thick films) and reversible, leading in the end to an equilibrium with the humidity of the environment. This effect results in a change in volume and modifies quite heavily the mechanical behaviour of PEDOT:PSS from brittle, in dry environment to plastic in wet environment. Lang et al. for instance reported a change of the Young's modulus from 2,8 GPa at 23% RH to 0,9 Gpa at 55% RH, and of the tensile strength from 53,2 MPa to 22,2 MPa in the same RH range[37], owing to PEDOT:PSS water uptake.[38]

Several attempts at modifying the standard thermal NIL protocols so as to cope with the peculiar thermo-mechanical behaviour of PEDOT:PSS have been reported. An approach consisted in carrying out the imprinting process under water saturation conditions, using water vapour like a plasticizer.[44] By this technique 40 nm height features with sub-100 nm critical dimension of a silicon stamp could be successfully reproduced into PEDOT:PSS. Another method, that consisted in placing with no additional load an elastomeric stamp with hydrophilic surface on a PEDOT:PSS film followed by annealing has been demonstrated for shallow structures (h=10 nm depth, 700 nm period grating).[45]

A different method consisted of pre-treating the PEDOT:PSS film for 24 h at low relative

humidity (15% RH), followed by a nanoimprint lithography step at 100 °C in ambient air (at 45% RH). This NIL process exploits the higher Young's modulus of PEDOTT:PSS with low water content, in order to avoid structures to be damaged during the demolding, yet sufficient plasticity to undergo deformation under pressure. Grating of lines of 70 nm in width and 60 nm in height, corresponding to an aspect ratio (AR) of 0.86 were reported in this case.[46] In all cases, only very shallow nanostructures could be obtained, a limitation that we intended to overcome.

Given the strong effect of RH on the PEDOT:PSS mechanical properties in the development of a nanoimprint lithography process here reported we have focused our attention on this parameter. Humidity was found to play a crucial role in the process, and high quality high aspect ratio nanostructures were reliably and reproducibly obtained in a process window at high RH, close to water vapour saturation. Surprisingly, the process of nanopatterning entails very strong effects on conductivity, work function and electronic states of the valence band. This fact may open new opportunities for tailoring PEDOT:PSS properties for specific optoelectronic applications.

2. Results and discussion

2.1 Water-Vapour-Assisted Nanoimprint Lithography

The peculiarity of the new Water-Vapour-Assisted NIL (WVA-NIL) process consists of taking advantage of the changes in the PEDOT:PSS thermo-mechanical properties induced by a controlled drop of RH in the atmosphere surrounding the sample, between stamp indentation and stamp release. In particular, during the indentation the PEDOT:PSS film should contain a sufficient amount of water to be soft and deformable at moderate temperature. On the contrary, small residual amount of water should be present during the stamp separation to benefit from a

higher PEDOT:PSS internal cohesion and from the shrinkage upon drying of the features. This last aspect results in a frictionless extraction of the stamp from the complementary features during demoulding.

The figure 1 shows the scheme of WVA-NIL process. PEDOT:PSS films are first prepared by spin-coating. The thickness investigated in this study ranges between 32 and 350 nm. For the deposition of "thick" layers (>50 nm) the starting commercial solution, the CLEVIOS P VP Al 4083, was pre-concentrated by partial evaporation of water (by hot stirring in air) and filtered with 450 nm pore diameter cellulose acetate filters.

After deposition, PEDOT:PSS film is equilibrated with the surrounding atmosphere, maintained at controlled relative humidity and at room temperature. The stamp is put face down onto the sample. Pressure is applied and the heating ramp is started. The RH set initially is maintained until the pre-set temperature for the imprinting process is reached. After a dwell time at these conditions the RH of the surrounding atmosphere is lowered. The PEDOT:PSS film, confined between substrate and stamp, dries from the edges inwards, which causes the shrinkage of the nanostructures. Finally, the plates are cooled down and the stamp is separated from the film/substrate. The fact that the drying starts from the edges and progress towards the centre of the sample does not result in any appreciable non-uniformity in the pattern quality nor in the physical properties of the film up to the tested samples size of 25x25 mm^2.

The above process scheme has been tested in a wide process parameters' window, i.e. in the range 0-100% of RH, 25°-150°C of temperature, and 2-12 MPa of pressure. The results obtained at fixed pressure of 10 MPa and for different temperatures and different RH are summarized in Figure 2. Imprinting tests at 0% RH (done in a nitrogen-filled glovebox) showed that no pattern at all could be obtained in the 25-150°C range, and only at temperature and pressure as high as ~250°C and ~60 MPa, respectively, PEDOT:PSS plastic deformation could take place (Figure 2(b), micrograph A), resulting anyhow in the formation of shallow structures. Moreover, at 0%

RH, 250°C and 60 MPa the presence of brittle fractures in the resulting structures was observed. In general, the width of the PEDOT:PSS features imprinted in dry conditions (0% RH) exactly reproduces that of the mould, which results in a friction force exerted during stamp separation. Conversely, to test the mechanical stability of dried PEDOT:PSS nanostructures (produced by WVA-NIL in humid environment and dried afterwards), we applied with the help of a flat stamp a pressure of 20 MPa at 0% RH and 150°C on a PEDOT:PSS grating. No deformation of the original structures was detected, which leads to the idea that nanostructured PEDOT:PSS films could serve themselves as stamps or could be permanently indented as nanopatterned electrodes into various conjugated materials. This would open a new strategy for the fabrication of organic optoelectronic devices with novel architectures.

At 25% RH, imprinting of PEDOT:PSS was found feasible. At 100 °C the imprinted features were shallow (Figure 2(b), micrograph B), while at 150 °C they appear fully indented (Figure 2(b), micrograph C). However, in the latter case, we did not detect any appreciable lateral shrinkage of the features, which leads to the build-up of friction forces between PEDOT:PSS and stamp during the demolding and explains why the resulting structures were partially damaged.

At 100% RH (i.e. vapour saturation), the PEDOT:PSS film becomes unstable, with a tendency to de-wetting, resulting in poor and irreproducible imprinting results. However, slightly below saturation (90-95% RH) the previous issues disappear. Nevertheless, at temperatures below 60°C the film could not be dried in a reasonable time, arbitrarily set to 30 min, and consequently the structures in the film were severely distorted or ripped away during demoulding (Figure 2(b), micrograph D).

A convenient process window in the (RH, T) plane, leading to features exceeding AR of 1 was identified in the approximately triangular region defined by the vertexes (40% RH, 150 °C), (95%

RH, 150 °C) and (95% RH, 80 °C). The imprinting processes of Figure 2(b), micrographs E, F, G, H, I were conducted in that region.

Structures of moderate aspect ratio (1<AR<2) were obtained at 95% RH and 80 °C (micrograph E), and 75% RH and 100 °C (micrograph F). Structures of increasing AR were obtained at 150 °C by increasing the relative humidity, from 55% (micrograph G) to 75% (micrograph H), and 95% (micrograph I).

The optimal WVA-NIL process parameters for the fabrication of high AR nanostructures is represented by the region at high RH and high temperature such as ~95% RH, ~150 °C and ~10 MPa (micrograph I). At these conditions the excellent plasticity of the material and the fast evaporation of water results in a relatively short process time, leading to high AR structures, easily and reliably separated from the stamp, owing to a shrinkage of up to 20-25% of the features' width.

The WVA-NIL process was extensively tested using different silicon stamps with features ranging from 80 to 250 nm, and height from 100 to 500 nm. In none of the tested imprinting conditions, even at temperatures and pressures of 200 °C and 30 MPa, the residual layer could be reduced below 20-30 nm.

2.2 Effects of WVA-NIL process on the physical properties of PEDOT:PSS

Having identified a convenient parameters' window for the water-vapour-assisted NIL process, the attention has to be focused on the effects that this process has on the PEDOT:PSS electronic properties, in particular on the conductivity, work function, and density of states in the valence band.

2.2.1 WVA-NIL effects on PEDOT:PSS conductivity

It is well known that PEDOT:PSS physical properties strongly depend on the relative amount of PEDOT and PSS, but that they can also be affected by the chosen processing conditions or by adding high boiling solvents (HBS) to the dispersion[47,48,49,50,51] Pettersson et al. revealed the effect of sorbitol on the refractive index and extinction coefficient.[48] Jönsson et al. found a 600-fold increase of conductivity and an increase by a factor of 2–3 of the ratio of PEDOT-to-PSS at the film surface by adding various solvents to the dispersion.[49] Kim et al. investigated the temperature-dependent conductivity of PEDOT:PSS doped with different solvents such as methyl sulfoxide (DMSO), N,N-dimethylformamide (DMF), tetrahydrofuran (THF), deducing that the screening effect of the solvent plays an important role in the variation of the conductivity.[52]

Other works highlighted the fact that the deposition by spin-coating itself introduces an anisotropy caused by the squeezing of PEDOT:PSS colloids orthogonally to the substrate, which results in different in-plane and out-of-plane conductivities.[53,42] The effect of exposing PEDOT:PSS to temperatures exceeding 100 °C in the presence of oxygen and/or moisture was reported to slowly degrade the conductivity.[54](Huang, Miller, de Mello, de Mello, & Bradley, 2003; Vitoratos et al., 2009) Given, the strong PEDOT:PSS susceptibility to fine processing an compositional details, it is important to establish how the physical properties of this material are affected by the different WVA-NIL processing conditions.

The first observed effect of our protocol was that conductivity is enhanced by the pre-concentration of PEDOT:PSS water dispersion. In fact, films spin-coated from the concentrated dispersion showed ~1 order of magnitude increase in the film conductivity compared to those deposited from the pristine dispersion (Figure 4a). This effect would be compatible with the

formation already in the pre-concentrated dispersion of larger PEDOT:PSS colloids, which, according to the PEDOT:PSS conductivity model by Vitoratos et al.[54] is expected to lead to larger conductivity values. However, even more pronounced was the effect arising from the WVA-NIL process. The conductivity was found to increase as a function of the RH. For WVA-NIL processes at high RH, enhancement by up to 5 orders of magnitude with respect to the pristine dispersion has been measured. This effect was limited to the areas actually compressed by the stamp, while areas not subjected to pressure were not affected. On the contrary, thermal NIL processes performed in glovebox (0% RH) left conductivity nearly unaffected. The effect on the conductivity depends also on the temperature at which the WVA-NIL process is carried out (Figure 4b). Conductivity does not change for process temperatures up to 80°C while it increases nearly exponentially, starting from ~100 °C. For all tested temperatures the conductivity was found to be independent of the applied pressure in the 2 to 12 MPa range. Only in the case of no load applied to the stamp, the conductivity showed only a weak, almost negligible increase, likely due to the ineffective confinement of the water vapour and the consequent faster drying of the film. This interpretation would also explain why WVA-NIL process performed with flat stamps results in an enhancement of conductivity exceeding that obtained with nanostructured stamps even if it does not involve any polymer flow. In fact flat stamps ensure a better water vapour confinement, while nanostructures provide easy paths for water escape. For given process parameters no major effect could be ascribed to the differences in the type and size of nanostructures (we varied AR from 1 to 5, for arrays or gratings of different periods). Only minor differences in the conduction were observed by measuring the resistivity in directions parallel and perpendicular to the lines.

The overall picture that emerges from the experiments is that the decrease of resistivity would not be related to any net polymer shear flow and consequent one-dimensional elongation of the PEDOT chains, but it would be an effect of "boiling" PEDOT:PSS in water. The understanding

of what the "boiling" of the film entails at the level of PEDOT:PSS microscopic morphology is beyond the scope of this work. We speculate that it may have a similar physical origin as that of the so-called high-conductivity PEDOT:PSS state caused by inclusion of high-boiling solvents (HBS) in the dispersion. In fact, water remaining confined by the stamp during the WVA-NIL process in PEDOT:PSS films at temperatures well above 100 °C, may play the role of plasticizer, similarly to high-boiling solvents such as sorbitol, providing the mobility to PEDOT and PSS to rearrange during the annealing.

On the other hand, the effect of the presence of high boiling solvents in the dispersion on morphology is still controversial. Several explanation schemes have been proposed. Some authors explain this phenomenon in terms of phase segregation between PEDOT and PSS due to the higher relative mobility of the chains of both components with interposed HBS.[55] Rearrangement of PEDOT-rich clusters into elongated domains, has been reported in STM studies.[56] Conformational changes of PEDOT:PSS toward linear filamentary structures [57,58] or screening due to the polar character of HBS[59] are also invoked to explain the increased conductivity. Future work is required to better understand the microscopic effects on morphology of WVA-NIL process and whether our hypothesis of an analogy with the effect induced by HBS holds.

2.2.2 Effects of WVA-NIL process on PEDOT:PSS work function and valence band states

Water-vapour-assisted NIL impacts also on PEDOT:PSS work function and on the states of the valence band. This fact is presumably correlated to a change in the phase segregation between PEDOT and PSS already reported by other studies[38,60] and in particular to a reduction in the PSS content at the surface.[61] In fact, the work of Lee et al.[61] establish a clear correlation between work function and surface concentration of the PSS dopant, with work function increasing for increasing PSS-to-PEDOT ratio at the surface. This effect was confirmed by our XPS

measurement (data presented in support information), in the opposite direction, i.e. a decreasing work function for decreasing PSS-to-PEDOT ratio.

We have analyzed such effects by Ultraviolet Photoelectron Spectroscopy (UPS). Figure 5a shows the valence band of a flat 160 nm thick PEDOT:PSS film on ITO (black spectrum) compared to that of films of the same thickness processed by WVA-NIL at 90% RH, but at different temperatures, namely, 80 ºC (blue spectrum) and 150 ºC (red spectrum). An additional treatment in oxygen plasma for 5 sec of the sample processed by WVA-NIL at 80 ºC leads to the green spectrum. The orange and yellow spectra refer to the sample processed at 150 ºC and subsequently treated in oxygen plasma for 5 sec and additional 15 sec, respectively. Figure 5b shows the measured work function of the same set of samples obtained by measuring the cut-off energy of the secondary peak.

The valence band spectrum of the as-deposited flat film (black spectrum) shows three main structures in the valence band in agreement with similar measurements already present in literature. In particular, the top of the valence band (peak centered at about 3 eV) can be extracted with a linear interpolation of the edge at about 2.41±0.05 eV from the Fermi level. The work function is 5.05±0.05 eV in good correspondence with the reported values in literature.[38,61,62]

In Figure 5a it is evident that the WVA-NIL treatment at 90 RH% and 150 ºC (red spectrum) strongly influences the valence band structures. Upon processing, all valence band peaks appear smeared out and the onset of the valence band shifts away from the Fermi level by about 2.9 eV (it is now at 5.27± 0.05 eV from the Fermi level). A concomitant decrease of the work function to about 3.53±0.05 eV is observed, corresponding to a shift of 1.52 eV from the value of the untreated film (black spectrum). Interestingly, by subsequent oxygen plasma (5 s and 20 s, orange

and yellow curves), the work function increases and valence bands appear to recover partially the lost structures with the edge shifting towards the Fermi level.

On the other hand, the NIL treatment at 90 RH% and 80 ºC (blue spectrum) only slightly modifies the valence band features with the top of the valence band at 2.44±0.05 eV from the Fermi level, very close to the value for the as-coated film. The work function decreases by less than 0.1 eV to 4.97±0.05 eV.

The oxygen plasma treatment on the WVA-NIL processed sample at 90 RH% and 80 ºC (green spectrum) slightly broadens the valence band features, but increases the work function at 5.21±0.05 more than the level of the as-coated film. Most interesting is the shift of the valence band onset edge that now appears closer to the Fermi level, i.e. 2.21±0.05 eV below it.

We try to rationalize the observed phenomenology based on the currently most accepted morphological model of the PEDOT:PSS system. This model depicts PEDOT:PSS morphology as consisting of colloids dispersed in water segregated into PEDOT-rich cores surrounded by PSS-rich shells, due to hydrophobic (hydrophilic) character of PEDOT (PSS). The core-shell structure is preserved to some extent also in the film. During the coating the colloids flatten into a lamellar structure of PEDOT-rich layers vertically alternated with PSS-rich ones.[42] PEDOT:PSS forms a surface layer that is highly enriched in PSS, with respect to bulk PSS/PEDOT ratio.[63,61] Furthermore, it is known that the work function correlates with the surface composition of the PEDOT:PSS film, which highly depends on the preparation processes such as thermal annealing process, solvent treatment and coating method.[62] In particular, higher PSS surface concentration leads to larger work function. [61]

Yun et al.[62] studied by UPS the electronic properties of PEDOT:PSS, reporting an increase of work function (from 5.0 to 5.2 eV) upon annealing for 1 h at 130 °C in ultra high vacuum (interpreted as the effect of desorption of contaminants), whereas for temperature higher than

170 °C the work function shifted gradually as a function of time towards lower values. For annealing temperatures of 220°C and 290 °C for 3 h the work function reduced to 4.8 and 4.5 eV, respectively, and this progressive lowering of work function as the annealing temperature increases, correlates with a progressive reduction of the PSS at the film surface, probed by XPS. On the other hand the work function of the only PEDOT (not doped by PSS) has been reported to be in the range 4.0 ±0.2 eV [64] or 4.3 eV.[65]

In our investigation on the WVA-NIL process the change of PEDOT:PSS work function was found, in the most dramatic case, much larger than previously reported studies on the effects of thermal annealing.[62] Interestingly, the work function in the WVA-NIL process carried out at 90% RH and 150 °C lead to a work function smaller even than the reported value for the undoped PEDOT (4.0 ±0.2 eV).

WVA-NIL, due to the confinement of water in the film while heating, ensures large relative mobility to the PEDOT and PSS chains. We presume that the lamellar structure of the PEDOT:PSS is disrupted and that a mixing at a finer level of the two components is reached, lowering the PSS content at the surface. The fact that the PSS-rich top surface is replaced by a phase more rich in PEDOT would explain the reduction in the work function.

2.3 Polymer photovoltaic cells on nanostructured PEDOT:PSS

We have investigated the impact that changes induced on the PEDOT:PSS electronic structure by WVA-NIL process and oxygen plasma produce on the J-V characteristics of poly(3-hexylthiophene) (P3HT) : indene-C_{60} bisadduct (ICBA) bulk heterojunction solar cells. By studying a series of solar cells on PEDOT:PSS anode buffer layers on ITO-coated glass either as spin-coated or processed by WVA-NIL (experimental details are in ESI), we observed that cells' characteristics are strongly correlated with the position of the conduction band edge and of the

work function of PEDOT:PSS. This dependence is so marked that the potentially favorable increase of conductivity by several order of magnitude induced on PEDOT:PSS owing to WVA-NIL process is totally obscured by the unfavorable shift of the alignment with the HOMO level of the P3HT.

Though the J-V characteristics that we report here do not represent the state of the art in organic photovoltaics, the relative trends in cells performances as a function of the WVA-NIL process parameters and oxygen plasma treatment on PEDOT:PSS reveal very significant information. The modest value of efficiency (~1%) is explained by the following reasons. Our devices were made in N_2–filled glovebox with ~50 ppm residual oxygen and water, and characterized in open atmosphere without encapsulation. Their active area of 26 mm^2 was significantly larger than that of the reported best performing ones, which rarely exceed 1-4 mm^2 area. In our experience as well as in published research by others[66] the efficiency of larger cells underestimates by a factor 2-3 the efficiency of the small-area cell limit, where the power dissipation in the ITO owing to ohmic loss is negligible. Finally, the large variability of P3HT-based bulk heterojunction solar cells from producer and from batch it is well known.[67]

In spite of these factors, the reported trends may be very relevant also in the case of high-efficiency cells.

Figure 6 shows the J-V characteristics and the main photovoltaic parameters, i.e. efficiency (η), short circuit current density (J_{sc}), open circuit voltage (V_{oc}) and fill factor (FF) under AM 1.5 simulated solar irradiation at 100 mW/cm^2 intensity. Measures are referred to a set of polymer solar cells made on 300 nm period PEDOT:PSS gratings (~120/180 nm lines/spaces) by WVA-NIL at 95% RH and temperatures of 80, 100, 130, and 150 °C .

The J-V characteristics of the cells made on PEDOT:PSS patterned by WVA-NIL differ markedly from the reference cell made on the as-deposited 160 nm thick PEDOT:PSS film.

We observe that the cell on PEDOT:PSS patterned at 80 °C and the reference one feature approximately the same efficiency of ~0.8%. However, the patterned one exhibits larger J_{sc} and V_{oc} than the reference cell (3.5 mA/cm^2 and 750 mV vs 2.5 mA/cm^2 and 650 mV, respectively) and lower FF (30% instead of 48%).

Increasing the WVA-NIL process temperature, which we saw previously to shift downwards the level of the PEDOT:PSS valence band edge, leads to a progressive reduction of J_{sc} ,V_{oc} and FF of the cells. In particular, the lowering of the work function from 5.05±0.05 eV to the 3.53±0.05 eV by processing the as-deposited flat PEDOT:PSS with WVA-NIL at 150 °C results in a reduction of cell efficiency from 0.8% down to 0.15%. The reason for this behaviour, in spite of the increased hole conductivity in the PEDOT:PSS, must be searched in the new position of the valence band that with increased WVA-NIL temperature moves below the HOMO of the blend (increasing, therefore, the barrier for hole injection from the polymer to the PEDOT:PSS).

Interestingly, the shift of the valence band edge and the reduction of the work function in PEDOT:PSS due to WVA-NIL process at high temperature and high RH can be reverted by a subsequent oxygen plasma treatment, that tends to shift the top of the valence band towards the Fermi level (Fig 5a). At the same time the efficiency of photovoltaic cells slightly increases (Fig. 7). Figure 7 shows the current-voltage characteristics and the extracted values for η, J_{sc}, V_{oc} and FF of OPV cells fabricated on PEDOT:PSS nanopatterned by WVA-NIL at 80°C and 95% RH. The pattern consisted of gratings of lines (250/250 nm lines/spaces) and were subsequently subjected to oxygen plasma for 0, 5, 30, 60 and 120 s.

On the other hand, the only WVA-NIL at 80 ºC leaves all valence band features almost unaffected as in the flat sample with the onset of the valence band at 2.44±0.05 eV from the Fermi level. The corresponding work function is 4.97±0.05 eV and the measured efficiency is about 0.8% as for the reference cell. The oxygen plasma treatment only slightly broadens the

valence band features, but increases the work function to 5.21±0.05 even higher than that of the reference sample. Most interesting is the shift of the valence band onset that now appears at 2.21±0.05 eV from the Fermi level, so reducing the barrier for the hole injection and consequently increasing the efficiency to 1.3%, i.e. 60% relative increase compared to the reference cell. By increasing the duration of the oxygen plasma to 1 min, the cells efficiency decreases to 1.1%, mainly due a drop in the current (whereas FF and V_{oc} remain essentially stable). Increasing further the plasma treatment to 2 min results in a drop to 0.7% efficiency by a combined drop of V_{oc} (from 800 mV to 525 mV) and FF (from 42.5% to 35%).

The observed trends as a function of WVA-NIL, temperature, and duration of oxygen plasma treatment show that the performances of cells tend to worsen for process conditions that increase the separation of the valence band edge with the Fermi level, possibly associated with the lowering of the work function.

In particular, the series of measurements as a function of the duration of oxygen plasma show an initial increase of efficiency for oxygen plasma etching of 5s, and 20s, according to the UPS measured shift of work function and valence band edge.

The results of this experiment agree with those of a study by Frohne et al.[68], who studied the influence of the anodic work function on the performance of organic solar cells. In that case, they used an ex-situ electrochemical procedure to alter the work function of PEDOT:PSS, adjusting the equilibrium potential E_q vs a standard electrode.[69] Frohne et al. showed that with decreasing E_q (i.e. decreasing work function) the J-V curves shifts progressively closer to the origin of axes, showing a progressive reduction in J_{sc}, V_{oc} and efficiency.[68]

Generally the doping of the PEDOT with PSS is associated also with a change in the optical properties of the material. This aspect has been investigated by UV-Vis photospectrometry, but no significant change in absorbance could be measured as the effect of WVA-NIL process.

3. Conclusions

We have systematically investigated a water-vapour-assisted nanoimprint lithography process for the patterning of PEDOT:PSS, exploring the space of parameter RH, p, and T. Relative humidity in the atmosphere surrounding the sample during the process of WVA-NIL plays a key role in the process. A reliable and reproducible nanoimprint lithography process has been developed, for the patterning of conductive PEDOT:PSS layers with lithographic results of unprecedented quality. It was found that the NIL process window lies in the region of temperature/relative humidity between 80 and 100 °C and 75 to 95%, where sub-100 nm features with aspect ratio up to 6 have been achieved.

The process affects the electronic properties of PEDOT:PSS. In particular conductivity can be enhanced approximately by 5 orders of magnitude, work function can be decreased down to 3.5 eV, and valence band edge shifts by up to 3 eV. This may represent an opportunity to use PEDOT:PSS also as a cathode and not just as anode in optoelectronic applications.

The possibility of tailoring PEDOT:PSS electronic properties has a strong impact in organic photovoltaic cells performance, and implications may be relevant to other type of devices for energy conversion or storage. The testing of the WVA-NIL processed PEDOT:PSS in organic photovoltaic cells showed a clear effect associated to the shift of work function and the shift of the edge of the valence band. In particular, a shift towards the Fermi energy of the valence band edge leads to an overall improvement of cells performance, while a shift in the opposite direction is associated to a worsening of the performance.

The availability of a patterning process for PEDOT:PSS and the mastering of its effects on key physical properties of the latter may open new opportunities in energy-related applications of conjugated materials.

4. Material and Methods:

Substrate preparation

PEDOT:PSS films were deposited on 3 different types of substrate, namely Si (100), chosen for its easy cleavage in the preparation of cross-view SEM samples for the characterization of the lithographic results, Si(100) with 200 nm of thermal SiO_2 layer for the measurement of the PEDOT:PSS conductivity, and OLED Grade ITO Coated Glass with 15 Ω/sq (Visiontek Systems Ltd) for the fabrication of photovoltaic cell and for UV-VIS absorbance measurement.

The substrates were all thoroughly cleaned in class 1000 clean room using the same procedure, consisting of 30 minutes sonication in demineralised water with a detergent, and the sequential dipping in hot acetone, IPA, and milli-Q water. After drying under nitrogen stream the cleaning procedure is concluded with oxygen plasma for 5 minutes to improve the wetting of the substrate by the aqueous dispersion of PEDOT:PSS. The cleaning is done and the substrate were used shortly after cleaning and oxygen plasma.

Pre-concentration of the PEDOT:PSS dispersion and spin-coating

The PEDOT:PSS films were produced by spin coating using a commercial aqueous solution of PEDOTT:PSS, "P VP Al 4083" from H.C. Starck, a low conductivity PEDOT:PSS commonly used for OPV for its good film forming properties. As the achievable films thickness range (30-70nm) was unsufficient for the patterning tests of high aspect ratio structures, the dispersion was pre-concentrated by partial evaporation of the water by magnetic stirring the solution in a glass vial open to air on a hot plate. The obtained dispersion is unstable at high pre-concentration levels (typically 50% volume reduction) and needs to be cooled down and rested for 24h in a

refrigerator to be stabilized, ensuring reproducibility in the thickness of the spin-coated films. Both pristine and pre-concentrated dispertions were used immediately after removal from the refrigerator (at 5°C), and filtered at the moment of the deposition with a 0,45 μm cellulose acetate filter. The spin coating was done by dropping the solution on the substrate already in rotation. The rotational speed was set between 1000 rpm to 3000 rpm depending on the final needed thickness. The film thickness reproducible within ±5nm as measured by profilometry.

Control of environmental humidity and sample handling

The samples were used either immediately after, or within 24 h from the spin-coating of PEDOT:PSS. In the latter case, the samples were maintained at the environmental humidity and were equilibrated with the WVA-NIL processing humidity for 5 minutes prior to the imprinting. The control of relative humidity was achieved by different means.

The imprinting tests at 0% RH were performed in a glove box fluxed with nitrogen. In the range between 25% and 75% RH was controlled by setting the desired value in a clean room equipped with active humidification/dehumidification system (in this case all steps from storage to positioning , imprinting and demoulding could be done at constant RH). For the high humidity tests in addition to setting high RH values for the cleanroom, the humidity was increased locally with an home-made bubbler, by fluxing nitrogen into milli-Q water, and delivering the water-saturated nitrogen in the gap between the press plates.

Nanoimprint Lithography

For WVA-NIL experiments a PW 20 E hydraulic press with heating plates (Paul-Otto Weber GmbH), with maximum heating and cooling rates of 8 °C/min and 50 °C/min and maximum force of 200 KN. An electronic pressure gauge ensure the control of pressure with 0.2 kN

resolution. For the experiments at 0% RH we used a home-made press with heating plates installed in glove box.

Stamps were silicon gratings of lines with periods of 180 nm, 250 nm, 300 nm, 500 nm, height between 90 and 250 nm period and duty cycle of 50%, or arrays of square or cylindrical holes in silicon of 180 and 500 nm period, respectively. Copies of the silicon stamps into Ormostamp (micro resist technology GmbH) on glass were used mainly for the patterning of PEDOT:PSS on ITO/glass, in order to solve a problem consisting in the disruption PEDOT:PSS features caused by the different thermal expansion of silicon stamps and ITO/glass substrates. By matching the thermal expansion of the substrates the previous problem disappeared. All stamps were surface functionalized by self-assembling of a monolayer of dodecyltrichlorosilane from vapour phase, to make their surface hydrophobic and ease the demoulding.

Oxygen plasma

Oxygen plasma treatment mentioned in the paper were performed with a 100W RF power on 6" cathode, pressure of $0.7x10^{-2}$ mbar and 115 V bias. For treatments of up to 30 seconds no significant change in the topography or in the conductivity were seen.

Conductivity measurement

The measurement of in-plane conductivity were made on as-coated, and WVA-NIL processed PEDOT:PSS films on SiO_2 (300 nm)/Si substrates. The WVA-NIL process was done using as a stamp either silicon gratings of lines, or flat silicon substrates. Contacts to PEDOT:PSS were made evaporation of 80 nm of gold by shadowing a stripe of the substrate with a calibrated metal wire, resulting in 220 μm gap between contacts, as measured by SEM. The resistance was obtained by a linear fit of the I-V curve between -2.0 V and 2.0 V. The conductivity for the

patterned films were measured in parallel and orthogonal direction with respect to the lines. To extract the conductivity we used the value of film thickness as measured by profilometry (before patterning the film).

Scanning electron microscopy

SEM images of the NIL or WVA-NIL-structured PEDOT:PSS films were acquired on a Zeiss Supra 40 scanning electron microscope. The cross-sections of the samples were obtained after few minutes drying PEDOT:PSS films on at hot plate at 150°C. Cleavage was done with the substrates still hot (cleavage without dehydration step lead to heavy plastic deformation of the PEDOT:PSS film).

UPS measurements

The UPS experiments were performed in a modified VG-II ESCAlab system (base pressure 10^{-10} mbar) using the He I radiation (21.22 eV). The electron hemispherical analyser worked with 2 eV of pass energy and the Fermi level was measured on the copper sample holder in electrical contact with the sample before each measurement. To obtain the work function relative to the measured Fermi level, a bias of 6.00 V was applied between the sample and the ground, in order to make visible the secondary photoelectron cut-off. The energy resolution was 50 meV.

OPV cell fabrication and testing

For cell production the PEDOT:PSS was deposited on patterned ITO substrate. The patterning of ITO was obtained by UV photolithography on the photoresist S1813 and wet etching of the ITO with a 10:10:1 $HCl:H_2O:HNO_3$ solution at 50-60°C. Regioregular poly(3-hexylthiophene) (P3HT) polymer used in this work was obtained from Rieke Specialty Polymers, Rieke Metals

Inc., while indene-C60 bisadduct (ICBA) from Lumtec Luminescence Technology Corp. After imprinting with Ormostamp/glass stamp, the PEDOT:PSS/ITO/glass samples were transferred in a nitrogen filled glove box. Residual water and oxygen were approximately 50ppm. Prior to device fabrication, a solution consisting of P3HT:ICBA in blend ratio of 1:1 (wt/wt %) and blend concentration of 40 mg/ml in dichlorobenzene was stirred at 40 ^{0}C for 36 hours inside glove-box. P3HT:ICBA solution was spin-casted onto the differently processed PEDOT:PSS films at 800 rpm for 50 seconds. Finally through shadow mask 100 nm thick aluminum contacts were vacuum evaporated at a pressure of approximately 2 x 10^{-6} Torr. After aluminum evaporation (with evaporator directly connected to glovebox) the devices were annealed at 140 ^{0}C for 30 minutes inside glove-box.

Figure Legends

Figure 1: *The water-vapour-assisted NIL process. Example of a cycle carried out at 80°C, 10 MPa and 95% RH.*

Figure 2: (a) WVA-NIL process window. Systematic experiments were made in order to determine the optimal process window. In the experiments, silicon stamps with array of holes or gratings were used, fixing the applied pressure and the duration to 10 MPa and 30 min respectively, and varying the imprinting temperatures and relative humidity. Lithographic results were characterized by SEM and the regions of the (T, RH) plane were qualitatively classified on the basis of the aspect ratio and integrity of the structures. The regions were classified as suitable for high aspect ratio (AR>1), for low aspect ratio (AR<1), not suited for imprinting, or characterized by stamp release issues (ripping-off of the structures or collapse during demoulding). (b) Scanning electron micrographs of nanoimprinted PEDOT:PSS structures obtained at different temperature and RH (and at fixed 10 MPa, with the exception of sample A), identified in the process window map (a) by capital letters. Imprinting at 0% RH, 250 °C requires high-pressure (60 MPa) to occur (A). Insufficient water content, 25% RH, leads to shallow indentation at 100 °C (B). or to brittle fractures at 150 °C (C). At 95% RH the structures imprinted at temperatures as low as 60 °C were severely distorted and ripped-off during demolding (D). Structures of moderate aspect ratio (1<AR<2) can be obtained at 95% RH and 80 °C (E), 75% RH and 100 °C (F), or 55% RH and 150 °C and (G). Structures of aspect ~2, such as the 180 nm period array of pillars with square cross-section shown in (H) were imprinted at 75% RH and 150°C. Lines of ~60 nm width and 400 nm height, corresponding to AR>6 in a 180 nm period grating were obtained at 95% RH and 150°C (I). Scale bars are 500 nm.

Figure 3: *Linear shrinkage of features' cross section as a function of the relative humidity set initially for the WVA-NIL process for lines and pillars imprinted at 10 MPa. No significant difference in the shrinkage was found for gratings of different period in the 180 – 500 nm range.*

Figure 4: *In-plane conductivity of PEDOT:PSS films as a function of* ***a)*** *the relative humidity and* ***b)*** *the temperature set for the WVA-NIL process. The data refer to 32 nm thick film (dashed red line) spin-coated from the pristine PEDOT:PSS dispersion and to 160 nm thick film (dashed violet line) deposited from the pre-concentrated solution. The conductivities of the as-coated films are confronted to those of films processed by water-vapour-assisted NIL on thick films (160 nm) using a flat silicon substrate as a stamp.* ***a)*** *Effect of RH on the conductivity of films imprinted at 150°C and 8 MPa, and varying RH, from 0% to 95%.* ***b)*** *Effect of imprinting temperature on conductivity of films imprinted with 250 nm period line gratings mould and flat silicon, at 8 MPa, 95% RH and different imprinting temperature in the 80 - 175 °C range. The lines are guides to the eye.*

Figure 5: *UPS spectra for the pristine and WVANIL/oxygen plasma processed films. a) Valence band and b) Edge of secondary electrons*

Figure 6: *Performance of P3HT:ICBA bulk heterojunction solar cells build on the pristine and WVA-NIL patterned PEDOT-PSS anode buffer layer. a) J-V characteristics b) efficiency and short circuit current density c) fill factor and open circuit voltage for cells prepared on PEDOT:PSS patterned at different temperatures.*

Figure 7: *Performance of P3HT:ICBA bulk heterojunction solar cells build on the pristine and WVA-NIL patterned PEDOT-PSS anode buffer layer at 80 °C and 95% RH as a function of an additional oxygen plasma treatment. a) J-V characteristics b) efficiency and short circuit current density c) fill factor and open circuit voltage for cells patterned PEDOT:PSS treated in oxygen plasma for different time.*

Figure 1 (Radivo et al.)

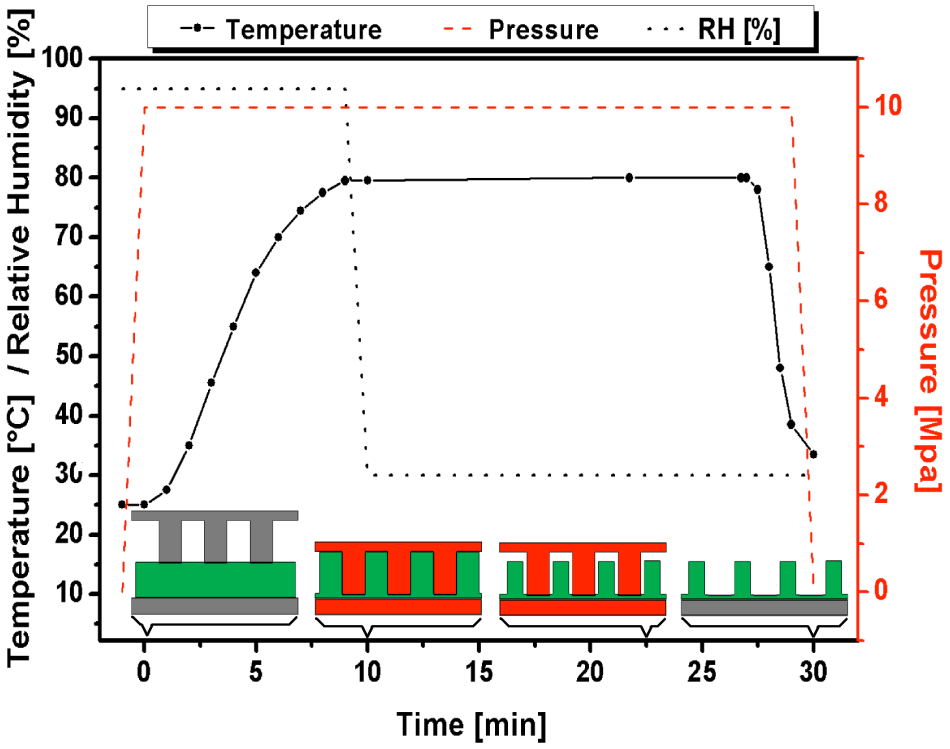

Figure 2 (Radivo et al.)

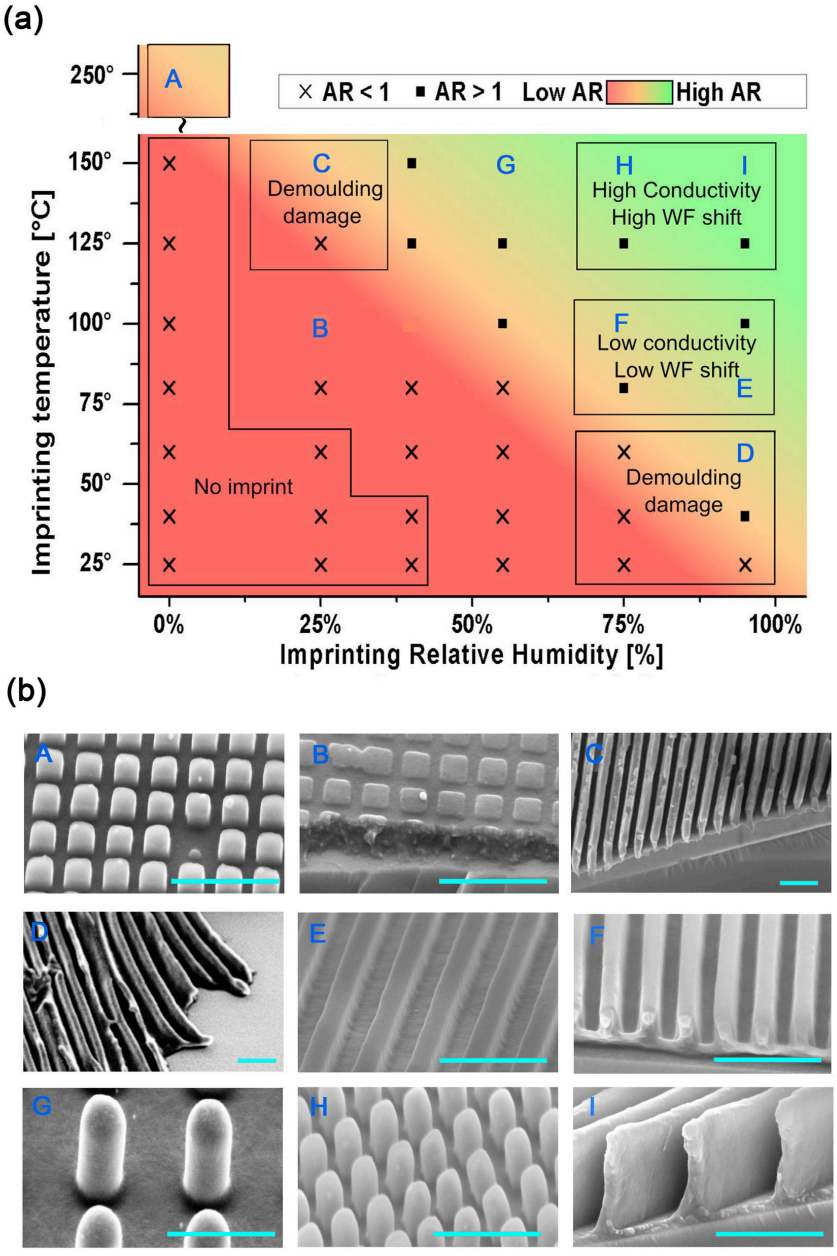

Figure 3 (Radivo et al.)

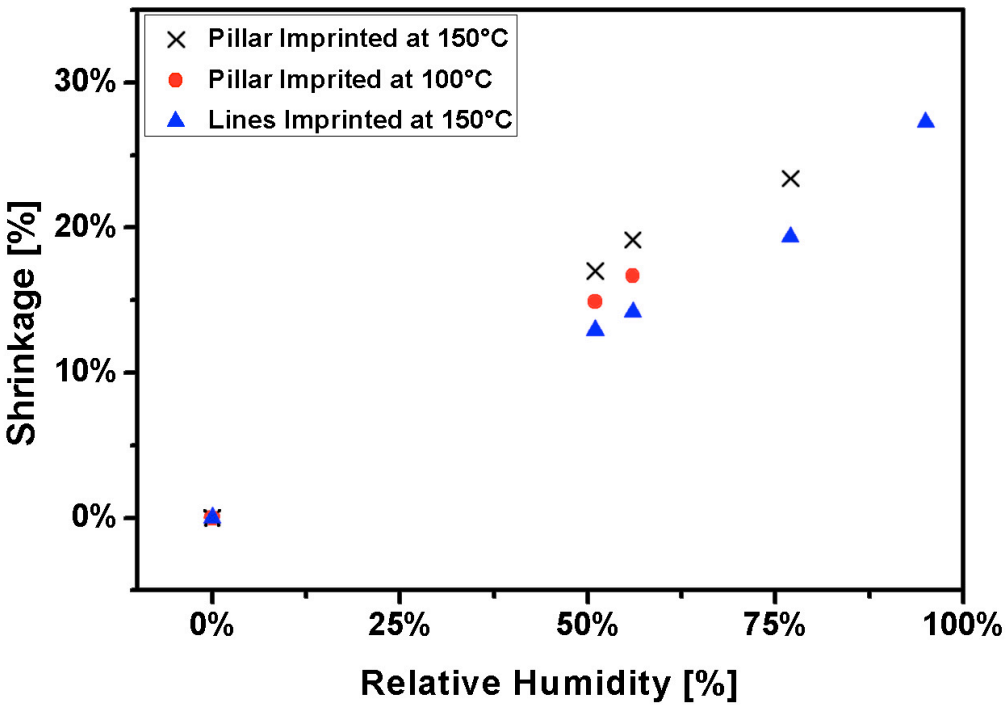

Figure 4 (Radivo et al.)

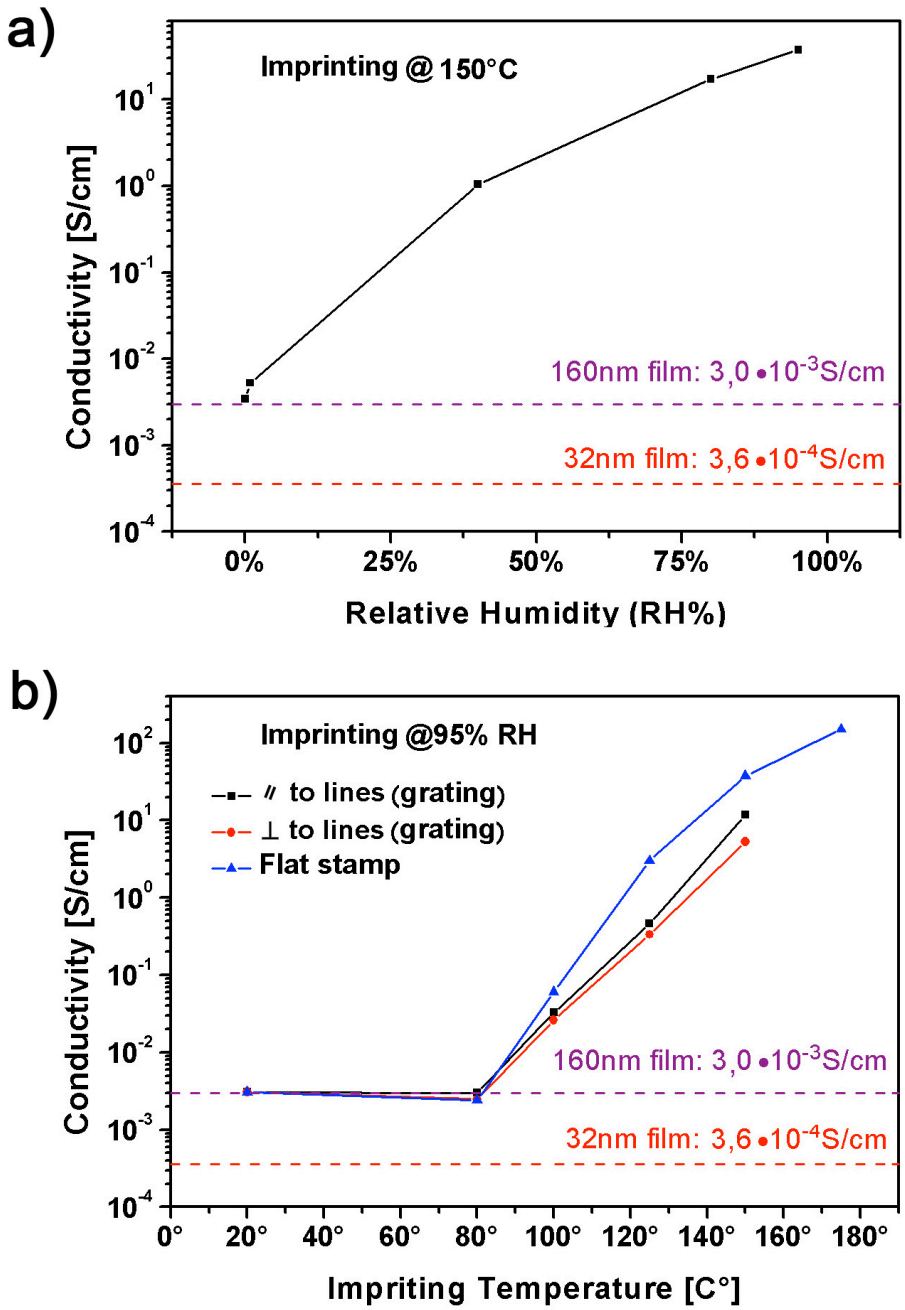

Figure 5 (Radivo et al.)

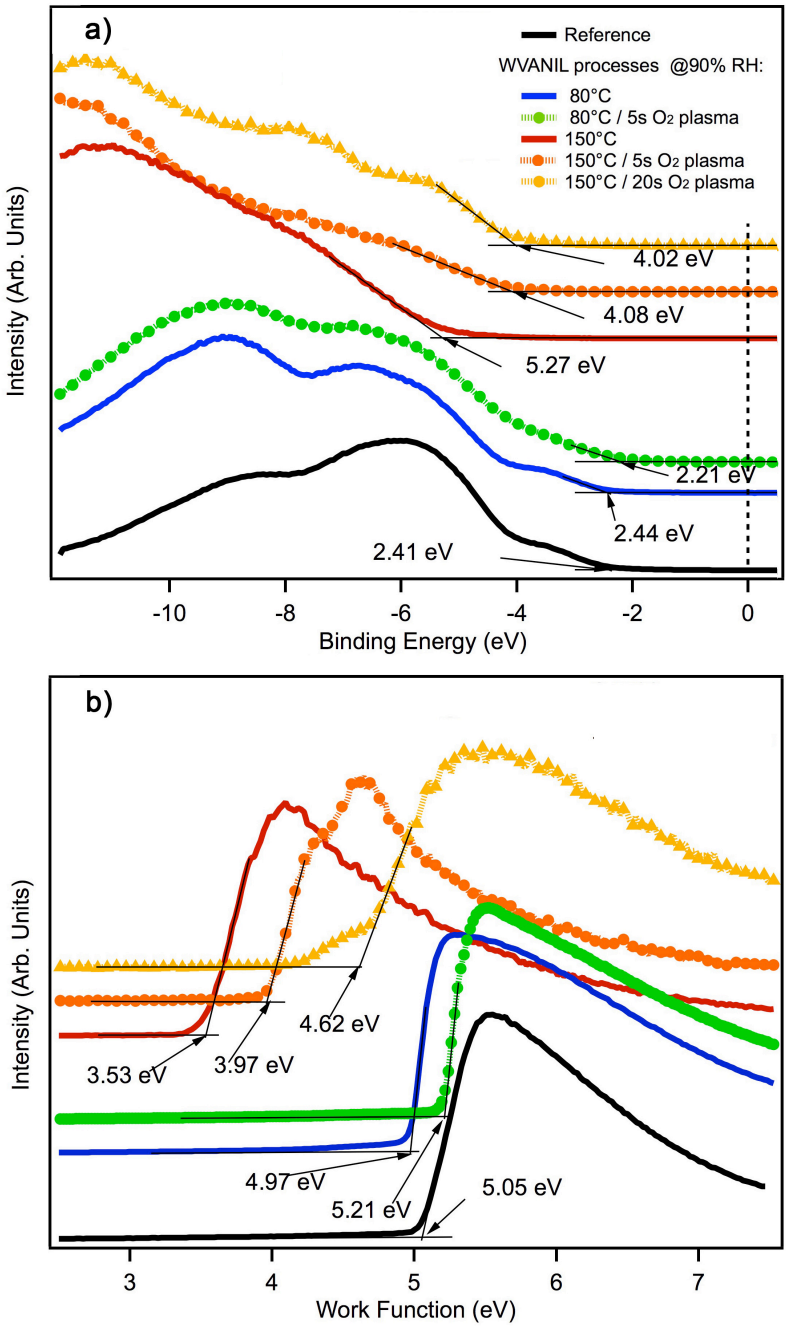

Figure 6 (Radivo et al.)

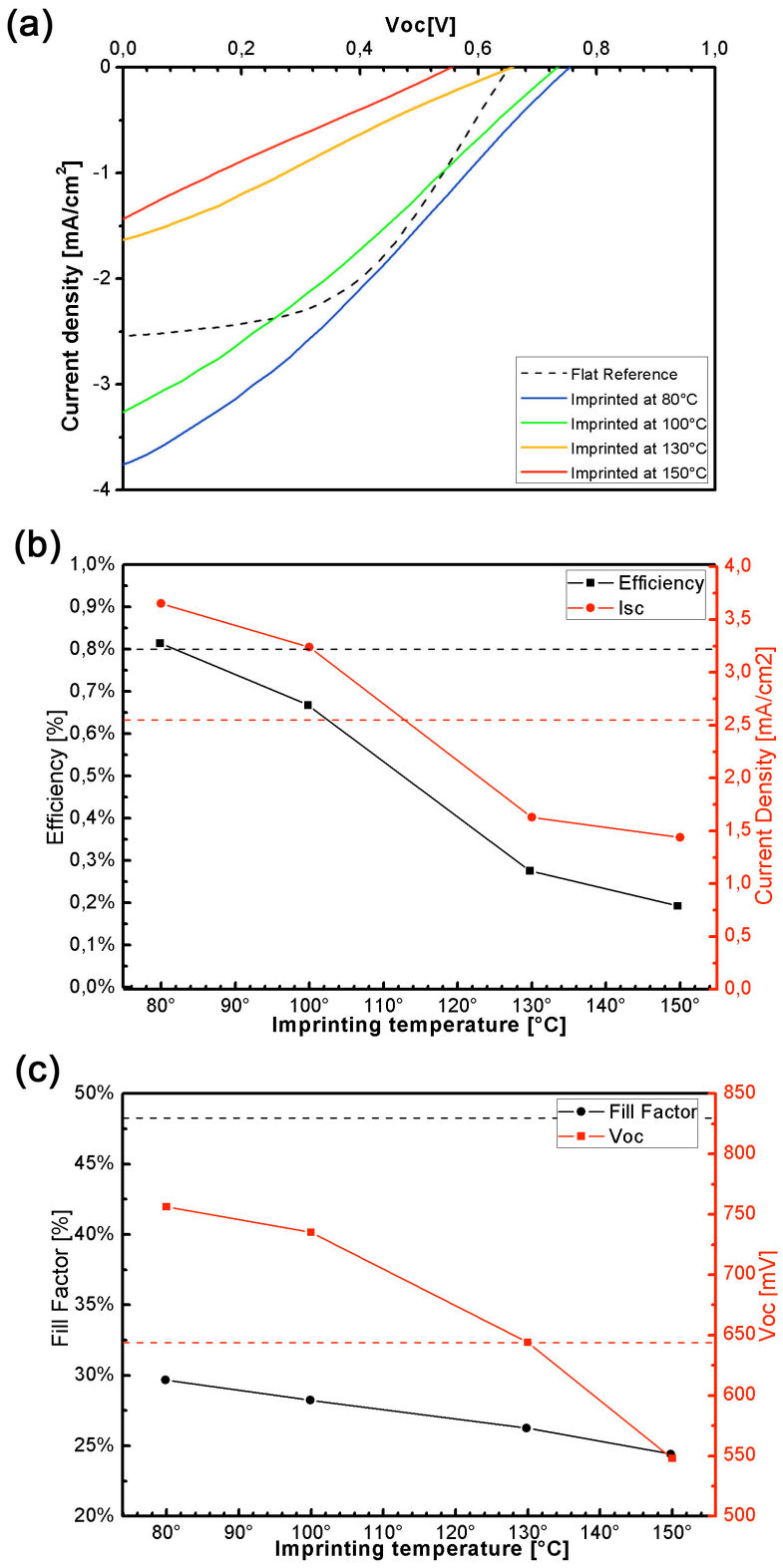

Figure 7 (Radivo et al.)

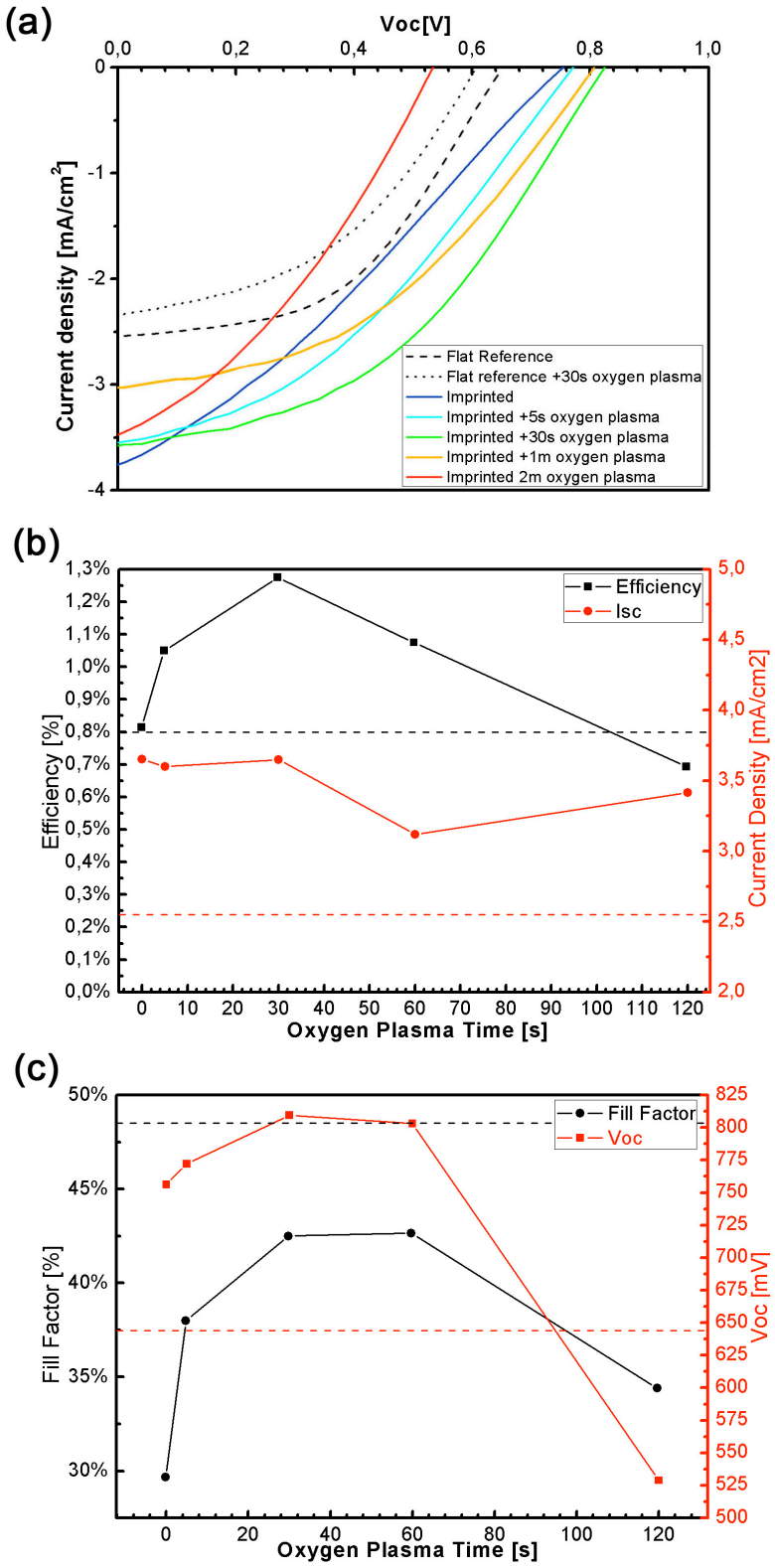

References

[1] S. Günes, H. Neugebauer, and N. Sariciftci, *Chemical reviews*, 2007, 107, 1324–38.

[2] K. Wang, H. Wu, Y. Meng, and Z. Wei, *Small (Weinheim an der Bergstrasse, Germany)*, 2014, 10, 14–31.

[3] S. Reineke, F. Lindner, G. Schwartz, N. Seidler, K. Walzer, B. Lüssem, and K. Leo, *Nature*, 2009, 459, 234–8.

[4] Crone, Dodabalapur, Lin, Filas, Bao, LaDuca, Sarpeshkar, Katz, Li, *Nature* **2000**, *403*, 521–3.

[5] S. Forrest, *Nature* **2004**, *428*, 911–8.

[6] G. Malliaras, R. Friend, *Physics Today* **2005**, *58*, DOI 10.1063/1.1995748.

[7] H. Klauk, U. Zschieschang, J. Pflaum, M. Halik, *Nature* **2007**,*445*, 745–8.

[8] H. Huitema, G. Gelinck, J. van der Putten, K. Kuijk, C. Hart, E. Cantatore, P. Herwig, A. van Breemen, D. de Leeuw, *Nature* **2001**, *414*, 599.

[9] Y. Xu, F. Zhang, X. Feng, *Small (Weinheim an der Bergstrasse, Germany)* **2011**, *7*, 1338–60.

[10] T. Kawase, H. Sirringhaus, R. H. Friend, T. Shimoda, *Advanced Materials* **2001**, *13*, 1601-5.

[11] P. Calvert, *Chemistry of Materials* **2001**, *13*, DOI 10.1021/cm0101632.

[12] D. A. Pardo, G. E. Jabbour, N. Peyghambarian, *Advanced Materials* **2000**, *12*, 1249-1252

[13] D. G. Lidzey, M. Voigt, C. Giebeler, A. Buckley, J. Wright, K. Böhlen, J. Fieret, R. Allott, *Organic Electronics* **2005**, *6*, 221–228, DOI 10.1016/j.orgel.2005.06.007.

[14] P. Watkins, A. Walker, G. Verschoor, *Nano letters* **2005**, *5*, 1814–8.

[15] F. Yang, S. Forrest, *ACS nano* **2008**, *2*, 1022–32

[16] J. Weickert, R. Dunbar, H. Hesse, W. Wiedemann, L. Schmidt-Mende, *Advanced materials (Deerfield Beach, Fla.)* **2011**, *23*, 1810–28.

[17] S. Mubeen, J. Lee, N. Singh, M. Moskovits, and E. W. McFarland, *Energy & Environmental Science*, 2013, 6.

[18] N. Singh, S. Mubeen, J. Lee, H. Metiu, M. Moskovits, and E. W. McFarland, *Energy & Environmental Science*, 2014, 7.

[19] Cho and S. Lee, *Accounts of chemical research*, 2008, 41, 699–707

[20] Y. Hou, Y. Cheng, T. Hobson, and J. Liu, *Nano letters*, 2010, 10, 2727–33

[21] D. Khodagholy, T. Doublet, M. Gurfinkel, P. Quilichini, E. Ismailova, P. Leleux, T. Herve, S. Sanaur, C. Bernard, and G. Malliaras, *Advanced materials (Deerfield Beach, Fla.)*, 2011, 23, H268–72.

[22] R. Po, C. Carbonera, A. Bernardi, N. Camaioni, *Energy. Environ, Sci.* **2011**, **4**, 285.

[23] S.-I. Na, S.-S. Kim, J. Jo, D.-Y. Kim, *Advanced Materials* **2008**, *20*, 4061–4067, DOI 10.1002/adma.200800338.

[24] S. K. Hau, H.-L. Yip, J. Zou, A. K.-Y. Jen, *Organic Electronics* **2009**, *10*, 1401–1407, DOI 10.1016/j.orgel.2009.06.019.

[25] B. Winther-Jensen, F. C. Krebs, *Solar Energy Materials and Solar Cells* **2006**, *90*, *123-132*, DOI 10.1016/j.solmat.2005.02.004.

[26] F. Guo, X. Zhu, K. Forberich, J. Krantz, T. Stubhan, M. Salinas, M. Halik, S. Spallek, B. Butz, E. Spiecker, T. Ameri, N. Li, P. Kubis, D. M. Guldi, G. J. Matt, C. J. Brabec, *Advanced Energy Materials* **2013**, *3*, 1062–1067, DOI 10.1002/aenm.201300100.

[27] Y. Xia, K. Sun, and J. Ouyang, *Energy & Environmental Science*, 2012, 5.

[28] W. Zhang, B. Zhao, Z. He, X. Zhao, H. Wang, S. Yang, H. Wu, and Y. Cao, *Energy & Environmental Science*, 2013, 6.

[29] P. Lane, P. Brewer, J. Huang, D. Bradley, J. deMello, *Physical Review B* **2006**, *74*, DOI 10.1103/PhysRevB.74.125320.

[30] C. Tengstedt, W. Osikowicz, W. R. Salaneck, I. D. Parker, C.-H. Hsu, M. Fahlman, *Applied Physics Letters* **2006**, *88*, DOI 10.1063/1.2168515.

[31] B. Charlot, G. Sassine, A. Garraud, B. Sorli, A. Giani, P. Combette, *Microsystem Technologies* **2012**, *19*, DOI 10.1007/s00542-012-1696-5.

[32] T. Granlund, T. Nyberg, L. S. Roman, M. Svensson, O. Inganäs, *Advanced Materials* **2000**, *12*, 269-273.

[33] D. Li, L. J. Guo, *Applied Physics Letters* **2006**, *88*, 063513, DOI 10.1063/1.2168669.

[34] S.-F. Tseng, W.-T. Hsiao, K.-C. Huang, D. Chiang, *Applied Physics A* **2012**, *112*, 41–47, DOI 10.1007/s00339-012-7172-3.

[35] F. C. Krebs, M. Jørgensen, K. Norrman, O. Hagemann, J. Alstrup, T. D. Nielsen, J. Fyenbo, K. Larsen, J. Kristensen, *Solar Energy Materials and Solar Cells* **2009**, *93*, 422–441, DOI 10.1016/j.solmat.2008.12.001.

[36] L. J. Guo, *Journal of Physics D: Applied Physics* **2004**, *37*, 123-141, DOI 10.1088/0022-3727/37/11/R01.

[37] U. Lang, N. Naujoks, J. Dual, *Synthetic Metals* **2009**, *159*, 473–479, DOI 10.1016/j.synthmet.2008.11.005.

[38] A. M. Nardes, M. Kemerink, M. M. de Kok, E. Vinken, K. Maturova, R. A. J. Janssen, *Organic Electronics* **2008**, *9*, 727–734, DOI 10.1016/j.orgel.2008.05.006

[39] R. Meier, C. Birkenstock, C. Palumbiny, P. Müller-Buschbaum, *Physical chemistry chemical physics : PCCP* **2012**, *14*, 15088–98.

[40] R. M. Reano, Y. P. Kong, H. Y. Low, L. Tan, F. Wang, S. W. Pang, A. F. Yee, *Journal of Vacuum Science & Technology B: Microelectronics and Nanometer Structures* **2004**, *22*, 3294-9, DOI 10.1116/1.1825013.

[41] L. Tan, Y. P. Kong, S. W. Pang, A. F. Yee, *Journal of Vacuum Science & Technology B: Microelectronics and Nanometer Structures* **2004**, *22*, 2486-92, DOI 10.1116/1.1800353.

[42] A. M. Nardes, M. Kemerink, R. A. J. Janssen, J. A. M. Bastiaansen, N. M. M. Kiggen, B. M. W. Langeveld, A. J. J. M. van Breemen, M. M. de Kok, *Advanced Materials* **2007**, *19*, 1196–1200, DOI 10.1002/adma.200602575.

[43] X. Crispin, S. Marciniak, W. Osikowicz, G. Zotti, A. W. D. van der Gon, F. Louwet, M. Fahlman, L. Groenendaal, F. D. Schryver, W. R. Salaneck, *Journal of Polymer Science Part B: Polymer Physics* **2003**, *41*, 2561-83, DOI 10.1002/polb.10659.

[44] Htay Hlaing, Xinhui Lu, Chang-Yong Nam, and Benjamin M. Ocko, *Small* **2012**, *8, 3443–3447*.

[45] J. B. Emah, R. J. Curry, S. R. P. Silva, *Applied Physics Letters* **2008**, *93*, DOI 10.1063/1.2973342.

[46] Y. Yang, K. Lee, K. Mielczarek, W. Hu, A. Zakhidov, *Nanotechnology* **2011**, *22*, 485301.

[47] W. H. Kim, A. J. Mäkinen, N. Nikolov, R. Shashidhar, H. Kim, Z. H. Kafafi, *Applied Physics Letters* **2002**, *80*, 3844-6, DOI 10.1063/1.1480100.

[48] L. Pettersson, S. Ghosh, O. Inganäs, *Organic Electronics* **2002,** 3, 143–148.

[49] S. K. Jönsson, J. Birgerson, X. Crispin, G. Greczynski, W. Osikowicz, A. D. van der Gon, W. Salaneck, M. Fahlman, *Synthetic Metals* **2003**, *139, 1–10*, DOI 10.1016/s0379-6779(02)01259-6.

[50] W. Zhang, B. Zhao, Z. He, X. Zhao, H. Wang, S. Yang, H. Wu, and Y. Cao, *Energy & Environmental Science*, 2013, 6.

[51] T. Takano, H. Masunaga, A. Fujiwara, H. Okuzaki, and T. Sasaki,*Macromolecules*, 2012, 45.

[52] J. Y. Kim, J. H. Jung, D. E. Lee, J. Joo, *Synthetic Metals* **2002**, 126, 311–316

[53] A. Nardes, M. Kemerink, R. Janssen, *Physical Review B* **2007**, *76*, 085208, DOI 10.1103/physrevb.76.085208.

[54] E. Vitoratos, S. Sakkapoulos, E. Dalas, N. Paliatsas, D. Karageirgopoulos, F. Petraki, S. Kennou, S. Choulis, *Organic Electronics* **2009**, *10*, 61–66, DOI 10.1016/j.orgel.2008.10.008.

[55] S. Timpanaro, M. Kemerink, F. J. Touwslager, M. M. D. Kok, S. Schrader, *Chemical Physics Letters* **2004**, *394*, *339–343*, DOI 10.1016/j.cplett.2004.07.035.

[56] A. M. Nardes, R. A. J. Janssen, M. Kemerink, *Advanced Functional Materials* **2008**, *18, 865–871* DOI 10.1002/adfm.200700796.

[57] J. Ouyang, Q. Xu, C.-W. Chu, Y. Yang, G. Li, J. Shinar, *Polymer* **2004**, 45, 8443.

[58] K. van de Ruit, R. I. Cohen, D. Bollen, T. van Mol, R. Yerushalmi-Rozen, R. A. J. Janssen, M. Kemerink, *Advanced Functional Materials* **2013**, DOI 10.1002/adfm.201301174.

[59] Y . Xia, J. Ouyang , *J. Mater. Chem.* **2011**, 21, 4927.

[60] B. Friedel, P. E. Keivanidis, T. J. K. Brenner, A. Abrusci, C. R. McNeill, R. H. Friend, N. C. Greenham, *Macromolecules* **2009**, *42*, DOI 10.1021/ma901182u.

[61] T.-W. Lee, Y. Chung, *Advanced Functional Materials* **2008**, *18, 2246–2252,* DOI 10.1002/adfm.200700766.

[62] D.-J. Yun, H. Ra, J. Kim, I. Hwang, J. Lee, S.-W. Rhee, J. Chung, *ECS Journal of Solid State Science and Technology* **2012**, *1, M10-M14,* DOI 10.1149/2.028201jss.

[63] G. Greczynski, T. Kugler, W. Salaneck, *Thin Solid Films* **1999**,*354*, 129-135, DOI 10.1016/s0040-6090(99)00422-8.

[64] K. Z. Xing, M. Fahlman, X. W. Chen, O. Inganäs, W.R. Salanek, *Synthetic Metals* **1997**, 89, 161-165.

[65] A. Gadisa, K. Tvingstedt, S. Admassie, L. Lindell, X. Crispin, M. R. Andersson, W. R. Salaneck, O. Inganäs, *Synthetic Metals* **2006**, *156, 1102–1107*, DOI 10.1016/j.synthmet.2006.07.006.

[66] A. K. Pandey, J. M. Nunzi, B. Ratier, A. Moliton, *Physics Letters A* **2008**, *372*, DOI 10.1016/j.physleta.2007.09.068.

[67] A. Ng, X. Liu, W. Y. Jim, A. B. Djurišić, K. C. Lo, S. Y. Li, and W. K. Chan, *Journal of Applied Polymer Science*, 2014, 131

[68] H. Frohne, S. Shaheen, C. Brabec, D. Müller, N. Sariciftci, K. Meerholz, *Chemphyschem : a European journal of chemical physics and physical chemistry* **2002**, *3*, 795–9.

[69] Gross, Muller, Nothofer, Scherf, Neher, Brauchle, Meerholz, *Nature* **2000**, *405*, 661–5.